Self-Calibration Technique for Junction Temperature Estimation of SiC MOSFET Inverters Loaded with Synchronous Reluctance Motors

Self-Calibration Technique for Junction Temperature Estimation of SiC MOSFET Inverters Loaded with Synchronous Reluctance Motors

Paolo Pescetto
Energy Department
Politecnico di Torino
Turin, Italy
paolo.pescetto@polito.it

Fausto Stella
Energy Department
Politecnico di Torino
Turin, Italy
fausto.stella@polito.it

Gianmario Pellegrino
Energy Department
Politecnico di Torino
Turin, Italy
gianamario.pellegrino@polito.it

***Abstract*— SiC devices have pushed the boundaries of power electronic conversion to new limits of power density and efficiency, but they also require appropriate thermal management. The conduction resistance of a SiC MOSFET is an indirect indicator of its junction temperature, provided that the R_{ON} versus temperature and current characteristic of the device is preliminarily mapped. Such R_{ON} map is normally obtained using dedicated test rigs, with the inverter connected to a custom inductive load. In this work, the R_{ON} maps of the power devices of a 3-phase Voltage Supply Inverter are obtained via self-calibration with the converter already connected to the target synchronous reluctance motor, without requiring rotor movements nor dedicated measurement equipment. The proposed procedure consists of a preliminary self-heating stage followed by R_{ON} mapping through current pulses along the zero-torque directions of the dq rotor reference frame. The connection to the target motor reduces the measurement domain in terms of maximum current and temperature with respect to the custom load. A polynomial model is used to extrapolate the R_{ON} characteristic out of the measurement domain, showing high estimation accuracy. Preliminary experimental results are presented.**

Keywords—TSEP, SiC MOSFET, Synchronous Reluctance Motor Drives, Junction Temperature Estimation, More Electric Aircraft, Reliability, Self-Commissioning, Online Junction Temperature Estimation

I. INTRODUCTION

SiC MOSFET power converters are gaining momentum in the automotive and aerospace sectors being now considered an obvious choice for high voltage (i.e. $V_{BUS} \geq 400\,V$) and high-current traction inverters [1], [2], [3]. SiC MOSFETs semiconductors are quickly replacing Si IGBT due to their lower specific conduction resistance (i.e. higher power density), lower switching losses and a purely resistive behavior without threshold conduction voltage (i.e. $0.7 - 0.8\,V$ for Si IGBT). This last feature enables to increase the efficiency of the converter in the low-power region, where traction inverters operate most of the time [4]. Furthermore, SiC devices have better thermal conductivity and can theoretically operate at much higher junction temperatures, thus having significantly lower cooling requirements [5], [6]. Also, this characteristic is particularly advantageous for the automotive industry where the converter must be able to operate in harsh environments with coolant temperatures that may approach $75°C$ [7]. Despite these favorable characteristics, reliability is still a major concern especially for safety critical applications such as automotive and aerospace.

It is well known from the literature that the junction temperature θ_j of a semiconductor plays a key role in defining its reliability [8], [9]. Therefore, θ_j must always be controlled and maintained under a certain limit to avoid the premature ageing of the semiconductor or at worst its immediate failure. However, the high-power density of such devices and their high specific cost (i.e., component oversizing is unacceptably expensive) make their thermal management even more critical than before. Advanced thermal management is required to fully exploit their superior power density while maintaining acceptable levels of reliability.

State-of-the-art power converters estimate the devices junction temperature θ_j by means of a thermoelectric model which allows to estimate the junction temperature rise with respect to the baseplate/heatsink whose temperature is usually monitored by means of a thermistor [11], [12], [13]. This indirect solution gives an approximated estimate of θ_j whose goodness depends on the accuracy of the thermo-electrical model. However, parametric dispersions between components of the same family and aging over time are difficult to model and most of the time they are overlooked leading to a rough estimate of the temperature.

Alternative solutions have been studied to measure or estimate the junction temperature of a semiconductor. Direct measurement techniques include the use of a thermal camera [15], [16] or a thermistor in direct contact with the die. The first one requires removing the insulating gel to provide visual access to the die, making its use relegated to a laboratory environment. Furthermore, the cost of the thermal camera may easily overcome the cost of the converter. The second one usually requires placing a thermistor as close as possible to the semiconductor die, however, galvanic insulation is critical, and the thermal impedance of the sensors combined with the fast thermal transients of the junction, usually causes attenuation and a delay in the measurement. On the market, there are few examples of devices embedding a sensor (thermistor or diode) for the direct measurement of the junction temperature [14]. In most cases, only one thermistor is used to monitor the housing temperature, which is often much lower than the actual junction temperature. Therefore, to overcome this problem over the years have been developed multiple techniques that use currents and voltages across the component as an indirect indicator of its junction temperature. Among the so-called thermo-sensitive electrical parameters [17]-[18], the correlation between the conduction resistance R_{ON} of the MOSFET and junction temperature is retained the most feasible and reliable. This technique is widely used in laboratory tests for design validation and thermal modelling purposes by identification of selected samples. However, it

does not yet find application in commercial converters due to unsolved challenges such as the need of calibrating the $\theta_j(i_{DS}, R_{ON})$ characteristic, which is unique for each device and changes with aging. A 3-phase SiC MOSFET converter capable of self-commissioning of the R_{ON} characteristics of the power devices and consequent junction temperature estimate has been previously presented in [18]. The functional block of the implemented temperature estimator is shown in Fig. 1. The conduction voltage and the current of each MOSFET are measured at each PWM period ($50\ \mu s$) during converter's operation and input to the respective temperature lookup table $\hat{\theta}_j(i_{DS}, R_{ON})$. In [18] the temperature LUTs (one per MOSFET) were obtained through a dedicated calibration test, which involves positioning the converter on a hot plate at a controlled temperature while being connected to a dedicated three-phase inductive load. This method was later improved in [19] where the calibration test was performed with the inverter directly connected to an induction motor. In that case, thanks to its isotropy, the induction motor was used as an equivalent three-phase inductor during the converter calibration phase.

This work furtherly extends the self-commissioning method to the more challenging case of a Synchronous Reluctance (SyR) motor drive. In this case, the machine can no longer be considered as a three-phase inductor as its exhibits different inductance values along its magnetic axes, and due to local saturation phenomena, these values are far from constant. A new and more advanced calibration test sequence is proposed to identify the R_{ON} characteristics without producing torque and shaft rotation during the standstill commissioning stage.

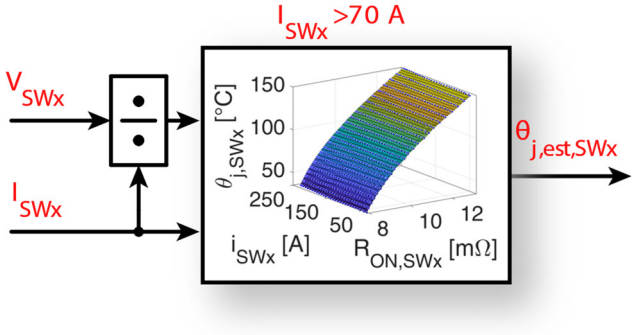

Fig. 1. Online junction temperature estimator functional block.

II. Experimental Set-Up

The proposed technique is validated on a three-phase prototypal inverter originally designed for a vehicle competing in the formula SAE student electric. An overview of the converter is shown in Fig. 2, while Fig. 3 depicts its schematic. As can be seen, it is a typical 2-levels 3-phase inverter, consisting of three half-bridge SiC power modules (ROHM BSM180d12p3c007) whose power ratings are reported in Tab.1. Each power module embeds two SiC power MOSFETs and two antiparallel SBD diodes thus improving the commutation performances. The inverter has been designed to operate at $20\ kHz$, with a maximum DC-link voltage of $800\ V$ and a maximum output current of 240 A (automatically reduced when the maximum junction temperature is reached). The inverter embeds all the circuitry (i.e. MCU, current and voltage sensing, gate driver, CAN communication and so on) to autonomously operate on the vehicle. Besides the standard measurements of the DC bus voltage, phase currents, and heatsink temperature, the conduction drain-source voltage of each switch is additionally measured, as shown in Fig. 3.

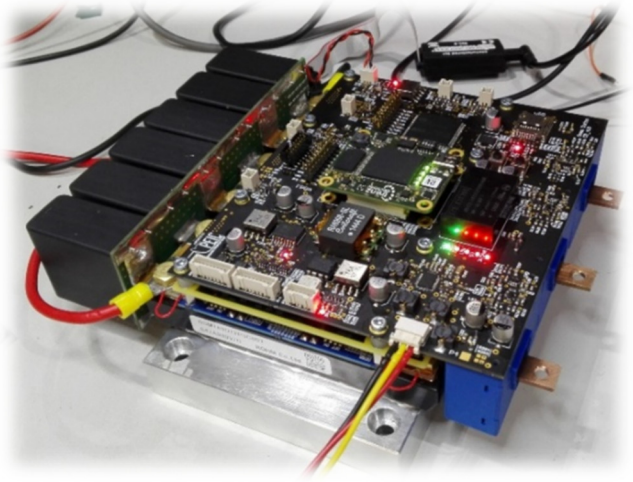

Fig. 2. Prototypal three-phase SiC inverter.

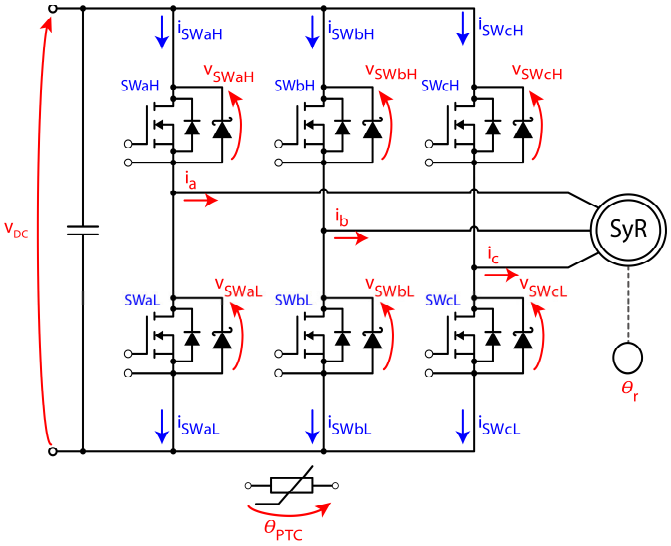

Fig. 3. Schematic of the power section of the three-phase SiC inverter showing in red the sampled quantities

Table I: Power Module Ratings

Manufacturer	ROHM
Model	BSM180D12P3C007
Configuration	Half Bridge
Rated current (θ_{case}=60°C)	180 A
Breakdown voltage	1200 V
R_{ON} @ 25°C,180A	10 mΩ
Max Junction Temperature	175°C

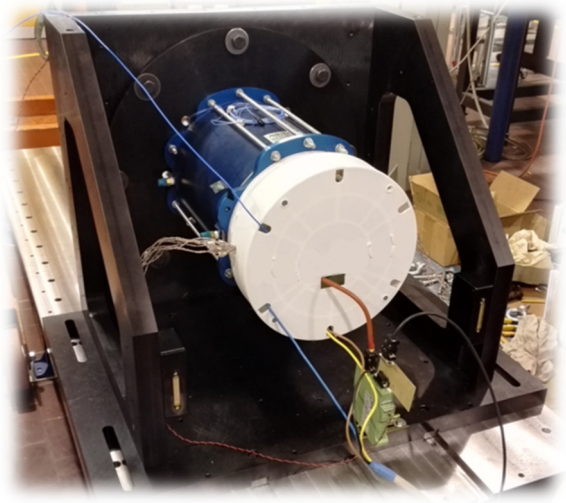

Fig. 4. SyR motor under test for aerospace applications.

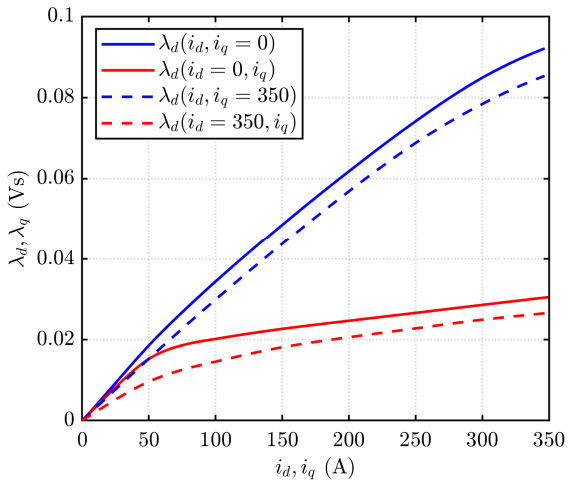

Fig. 5. Flux maps of the SyR motor under test.

Table II: SyR Motor Ratings

Rated power	250 kW
Rated frequency	333 Hz
Rated Torque	240 Nm
Rated Voltage	600 V_{DC}

To validate the proposed technique the inverter was connected to a 250 kW 3-phase Synchronous Reluctance (SyR) motor prototype, designed to serve as a starter-alternator for aerospace applications [20]. The machine picture is reported in Fig. 4, while Tab. II details its main specifications. The motor is equipped with a resolver for rotor position measurement. It should be noted that, as detailed in Section III, no torque or shaft rotation is produced during the commissioning stage, so the motor can either be connected to its mechanical load or not without affecting the results. Moreover, the inverter current and voltage transducers are employed, avoiding dedicated measurement equipment. In turn, the proposed technique for R_{ON} mapping and θ_j online estimation does not require any additional equipment with respect to the drive itself, regardless of the mechanical connection of the motor.

III. Proposed Calibration Test

The R_{ON} calibration test to obtain the temperature law consists of three main stages: a) self-heating, b) current pulses injection, and c) extrapolation of the R_{ON} characteristics. Each stage is detailed hereafter.

A. Self-heating

First, the converter heatsink needs to be heated. In order to avoid an external heating system, a self-heating procedure has been developed, where the heatsink is heated by the inverter losses. In the meantime, it is required to avoid motor rotation or relevant torque production.

To this aim, an open-loop I-Hz control has been implemented, imposing a rotating current vector to the SyR machine, with the inverter cooling system off. The AC current permits distributing the losses between the six MOSFETs equally. Since the motor is at standstill, such I-Hz control produces an alternated pulsating torque. Anyway, The current amplitude ($70\ A$) and frequency ($200\ Hz$), were chosen in order to avoid rotor movements. In the motor under test, the peak torque obtained during the self-heating stage is lower than 0.01 p.u.

For thermal characterization purposes, the self-heating temperature should be increased as much as possible, as it defines the temperature measurement domain of R_{ON} maps commissioning. Anyway, it should be noted that at this stage, the junction temperature is still not monitored. Therefore, the self-heating stage is automatically stopped once the heatsink thermistor outputs $85°C$, to avoid the risk of overheating the MOSFETs. Note that the heating current is relatively low ($0.3\ p.u.$) thus ensuring that the maximum junction temperature of the semiconductor is not exceeded even when the heatsink temperature reaches $85°C$. According to the semiconductor datasheet under these testing conditions, the junction over temperature with respect to the heatsink should be below $30°C$.

B. Current Pulses Injection and LUT data collection

Once the self-heating stage is terminated, the PWM modulation is disabled, and the inverter starts cooling naturally. During this first phase which takes ≈ 2 minutes, the junction temperature of the semiconductors becomes equal to that of the heatsink.

When the heatsink temperature decreases to $80\ °C$, the first sequence of current pulses is launched. Each sequence

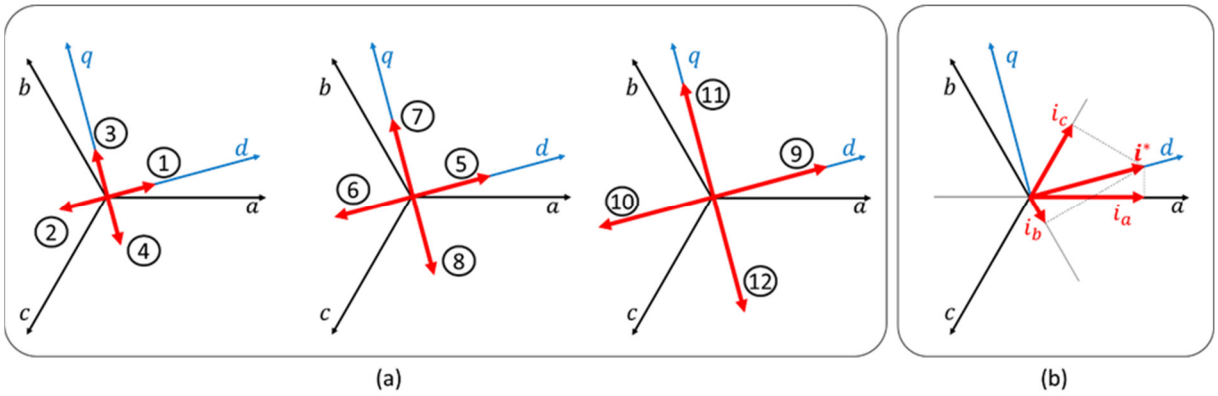

Fig. 6. (a) Current pulse sequence along the d and q axes of the SyR machine. (b) Resulting inverter phase currents caused by a pulse along the d axis of the SyR machine.

consists of a series of short current pulses of growing amplitude imposed by the inverter to the motor. For each current amplitude, four pulses are injected in positive and negative d and q directions of the machining, to avoid producing torque in the SyR motor and, at the meantime, equally excite the upper and lower MOSFETs in the inverter. It should be noted that, for each current pulse, the corresponding phase current is given by the projection of the dq current along the a, b and c directions, as depicted in Fig. 6 b). The full sequence of pulses in dq coordinates, for a given temperature, is reported in Fig. 7, while Fig. 8 reports the corresponding phase currents. After the first current pulse set, which takes a couple of seconds, the heatsink continues to cool down naturally. When the temperature of the heatsink drops by an additional 2.5 °C a new sequence of current pulses is injected by the inverter to the motor.

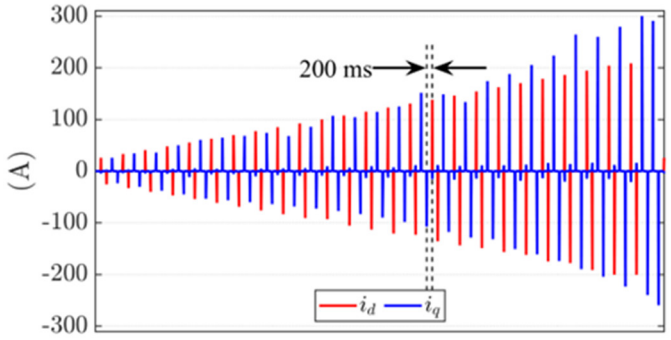

Fig. 7. Current pulses sequence in $\boldsymbol{dq}$ axes.

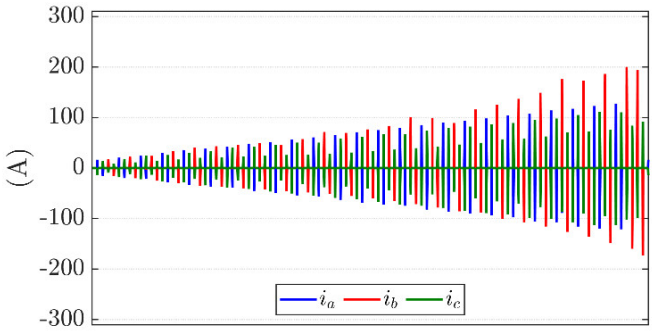

Fig. 8. Current pulses sequence in $\boldsymbol{abc}$ phase axes for θ=30°.

Each sequence of current pulses is meant to map the semiconductors at a specific temperature. This operation is repeated until the heatsink approaches room temperature (e.g. at 35°C). At this point, the identification is terminated.

For each pulse, the currents i_{SWx} and the voltages v_{SWx} across each switch are stored, and the corresponding R_{ONx} is computed:

$$R_{ONx} = \frac{v_{SWx}}{i_{SWx}} \tag{1}$$

Thanks to the short duration of the single current pulse ($150\ \mu s$) and the long pause between two consecutive pulses ($200\ ms$) the measured heatsink temperature θ_{PTC} is practically equal to the junction temperature θ_j during the pulse. Therefore, each current pulse provides a point in the $R_{ON}(\theta_j, i)$ characteristic.

C. Measurement Domain and Extrapolation of the R_{on} Characteristic

A similar current pulse sequence was previously adopted in [18], with the inverter connected to a custom inductive load and the heatsink externally heated with a heating plate at a controlled temperature. This permitted a full exploration of the operating domain in terms of junction temperature and phase current. In the present case, differently to [18], the direct connection of the inverter to the target SyR motor limits the temperature and current ranges of inspection, thus requiring dedicated post-processing of the collected data.

The temperature range of inspection is limited by the self-heating procedure, which only permits reaching a maximum temperature of 85 °C. As mentioned in Section III.A, this avoids the coolant to reach its boiling temperature and avoids damaging the MOSFETs during the heating stage, when θ_j is not yet monitored. At the end of the heating stage, an idle time is left to permit a uniform temperature distribution over the heatsink, further limiting the maximum measurement temperature at 80 °C. The identification stage terminates when θ_{PTC} approaches the room temperature, thus defining the lower limit of the measurement domain.

As described in Section III.B, the current pulses are given in the motor dq axes to avoid torque production, vibrations, and shaft movement. Moreover, the pulse duration is limited to 150 μs, i.e. three PWM periods T_{SW}, to avoid heating the MOSFETs during the pulse. The first two PWM cycles are

used to increase the current up to the target value while during the third one the data are sampled. Therefore, the DC-link voltage V_{dc} and motor inductances L_d , L_q define the maximum d and q current pulses amplitude.

$$\begin{cases} |i_d| \leq \frac{2}{3} \cdot \frac{V_{dc} \cdot 2T_{SW}}{L_d} \\ |i_q| \leq \frac{2}{3} \cdot \frac{V_{dc} \cdot 2T_{SW}}{L_q} \end{cases} \quad (2)$$

As depicted in Fig. 6 b), for each pulse the corresponding phase current is given by the projection of the current vector $\boldsymbol{i_{dq}}$ over the abc directions. Therefore, the maximum phase currents (same as MOSFETs currents) are given by:

$$\begin{cases} |i_a| \leq \max\left(|i_d \cos(\theta)|, |i_q \sin(\theta)|\right) \\ |i_b| \leq \max\left(\left|i_d \cos\left(\theta - \frac{2\pi}{3}\right)\right|, \left|i_q \sin\left(\theta - \frac{2\pi}{3}\right)\right|\right) \\ |i_c| \leq \max\left(\left|i_d \cos\left(\theta + \frac{2\pi}{3}\right)\right|, \left|i_q \sin\left(\theta + \frac{2\pi}{3}\right)\right|\right) \end{cases} \quad (3)$$

It should be noted that the three phases present different current limits, and each of them depends on the rotor position θ, which is random at the commissioning stage.

Upon data collection, the R_{ON} characteristic as a function of the die temperature θ_j and drain current i_{DS} is interpolated using the polynomial function (4):

$$\hat{R}_{ON}(\theta_j, i_{DS}) = R_0 + k_{\theta 1} \cdot \theta_j + k_{\theta 2} \cdot \theta_j^2 + k_i \cdot i_{DS} \quad (4)$$

Linear Least Square (LLS) regression [21] is adopted to retrieve the four parameters R_0, $k_{\theta 1}$, $k_{\theta 2}$ and k_i. This fitting function demonstrated to well represent the real R_{ON} characteristic [19], and it can extrapolate the data up to the maximum operating current and temperature even if based on a limited measurement domain. It should be noted that, differently from [18], the dq pulses excitation of the machine produces different current samples in the three phases. Moreover, the LLS algorithm necessarily operates on scattered data sets. Once the LLS algorithm estimates the model parameters R_0, $k_{\theta 1}$, $k_{\theta 2}$ and k_i for each of the six MOSFETs, the model in (4) is analytically reversed:

$$\hat{\theta}_j(R_{on}, i) = \frac{-k_{\theta 1} + \sqrt{k_{\theta 1}^2 - 4k_{\theta 2}(k_i i + R_0 - R_{on})}}{2k_{\theta 2}} \quad (5)$$

This last equation is adopted for online estimating the junction temperature of each switch during inverter operation, on varying its measured resistance and current.

IV. Experimental Results

To validate the proposed commissioning test, the MOSFETs temperatures are estimated while the inverter outputs a 3-phase sinusoidal current at 0.5 Hz, 220 A in Fig. 9 and 1 Hz, 220 A in Fig. 10. The temperatures of the six inverter MOSFETs are real-time estimated using the **full inverter maps** and the **reduced inverter maps**.

The full inverter maps are obtained from the calibration test with the hotplate and the inverter connected to a three-phase inductor, thus enabling to experimentally map the MOSFETs on the whole operating range without performing any extrapolation as shown in [18]. These maps can be considered as correct, as this methodology was previously validated against the thermal camera [22]. On the contrary, the reduced inverter maps are obtained with the inverter connected to the SyR motor without using an external plate. These testing conditions enable to experimentally map the MOSFETs only on a limited operating range (i.e. maximum temperature $80°C$ and maximum current depending on the rotor position). The maps outside the measurement domain are then extrapolated as illustrated in the previous sections.

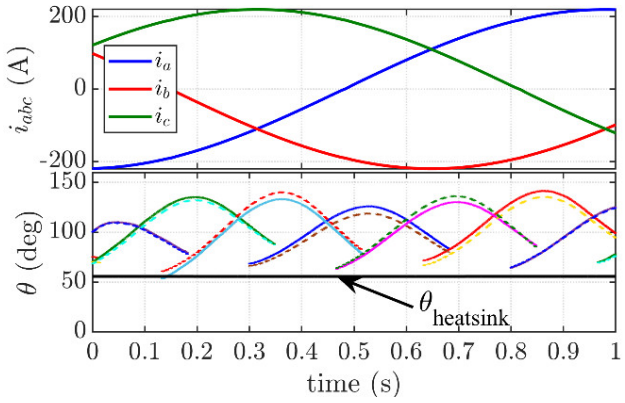

Fig. 9. Phase currents and (Bottom) estimated temperatures of the six power MOSFETs using the full inverter maps (continuous) and the reduced inverter maps (dashed). **Fundamental phase current 220 *Apk* and 0.5 *Hz***.

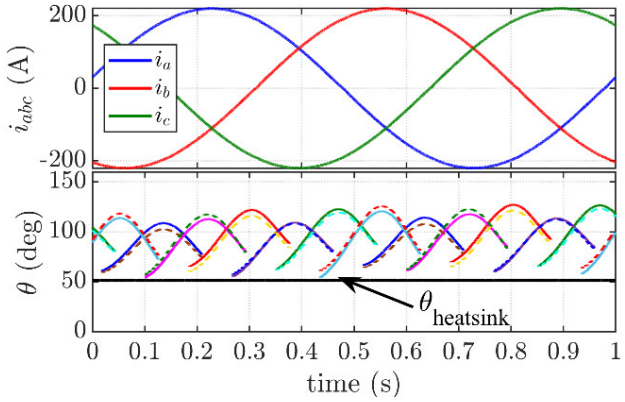

Fig. 10. Phase currents and (Bottom) estimated temperatures of the six power MOSFETs using the full inverter maps (continuous) and the reduced inverter maps (dashed). **Fundamental phase current 220 *Apk* and 1 *Hz*.**

In Fig. 9 the top plot shows the inverter phase currents while the bottom one shows the heatsink temperature measured with the thermistor and the estimated junction temperatures of the six inverter switches. The junction temperature estimations represented by the continuous line are obtained using the full inverter maps while the ones represented by the dashed line are obtained using the reduced inverter maps. The reduced maps present a good match with the full maps, and in this specific working condition, the error in the temperature estimation is below $5°C$. We can also see that while the junction temperature is affected by large thermal swings the heatsink temperature remains circa constant due to its large thermal constant. Therefore, the heatsink temperature cannot be considered representative of the junction temperature. In the provided results the junction temperature of the devices is estimated only at high levels of currents (i.e. $i_{DS} > 70\ A$). In fact, at low current levels the conduction

voltage of the MOSFETs is few mV making impossible to accurately measure its conduction resistance. However, the low current condition is not thermally critical. Furthermore, the junction temperature of the device is not estimated for $i_{DS} < 0$. In this case part of the current is conducted by the antiparallel diode, making it impossible to estimate the junction temperature of the MOSFET. However, this case is not thermally critical for two reasons: 1) the phase current is shared between the MOSFETs and the diode, therefore the MOSFET must sustain only a part of the conduction losses, 2) when $i_{ds} < 0$ the MOSFET operates in soft switching.

If we compare Fig. 9 (220 Apk AC current at 1 Hz) and Fig. 10 (220 Apk AC current at 0.5 Hz), we can clearly see that for the same heatsink temperature, the maximum temperature of the semiconductors tends to lower. This is due to the thermal inertia of the semiconductors that act as a low-pass filter on the temperature.

V. Conclusions

The direct mapping of R_{ON} for temperature estimation of SiC MOSFETs has been proposed for SyR motor drives. The challenges related to the use of the SyR machine, including the strong inductance variation with signal injection direction and amplitude while avoiding torque production have been addressed. Collected data on a limited calibration range have been extrapolated to cover the converter's operational domain. The experimental results show that extrapolated LUTs guarantee a temperature error within 5°C. The ability to perform the calibration test with the inverter connected to the target motor is of paramount importance for obtaining a reliable temperature estimation during the lifetime of the converter. In fact, it is well known from the literature that while the components age, their conduction resistance tends to increase therefore a new calibration test is required [23]. The proposed calibration test can be performed automatically during the idle time of the converter without the need for external intervention. i.e. After a certain number of working hours a new calibration test can be performed thus obtaining a new set of maps. Furthermore, if the old maps are compared with the new ones it is possible to have an indication of the ageing of the power semiconductor and use this information for prognostic [23], [24].

References

[1] J. Reimers, L. Dorn-Gomba, C. Mak, and A. Emadi, "Automotive Traction Inverters: Current Status and Future Trends," *IEEE Transactions on Vehicular Technology*, vol. 68, no. 4, pp. 3337–3350, Apr. 2019.

[2] T. M. Jahns and H. Dai, "The past, present, and future of power electronics integration technology in motor drives," *CPSS Transactions on Power Electronics and Applications*, vol. 2, no. 3, pp. 197–216, Sep. 2017.

[3] I. Husain et al., "Electric Drive Technology Trends, Challenges, and Opportunities for Future Electric Vehicles," *Proceedings of the IEEE*, vol. 109, no. 6, pp. 1039–1059, Jun. 2021.

[4] K. Olejniczak et al., "A 200 kVA electric vehicle traction drive inverter having enhanced performance over its entire operating region," in *2017 IEEE 5th Workshop on Wide Bandgap Power Devices and Applications (WiPDA)*, Oct. 2017.

[5] T. Zhao, J. Wang, A. Q. Huang, and A. Agarwal, "Comparisons of SiC MOSFET and Si IGBT Based Motor Drive Systems," in *2007 IEEE Industry Applications Annual Meeting*, Sep. 2007, pp. 331–335. doi: 10.1109/07IAS.2007.51.

[6] L. Zhang, X. Yuan, X. Wu, C. Shi, J. Zhang, and Y. Zhang, "Performance Evaluation of High-Power SiC MOSFET Modules in Comparison to Si IGBT Modules," *IEEE Transactions on Power Electronics*, vol. 34, no. 2, pp. 1181–1196, Feb. 2019.

[7] S. Jones-Jackson, R. Rodriguez, Y. Yang, L. Lopera, and A. Emadi, "Overview of Current Thermal Management of Automotive Power Electronics for Traction Purposes and Future Directions," *IEEE Transactions on Transportation Electrification*, vol. 8, no. 2, pp. 2412–2428, Jun. 2022.

[8] H. Wang, M. Liserre, and F. Blaabjerg, "Toward Reliable Power Electronics: Challenges, Design Tools, and Opportunities," *IEEE Industrial Electronics Magazine*, vol. 7, no. 2, pp. 17–26, Jun. 2013.

[9] F. Stella, G. Pellegrino, and E. Armando, "Coordinated On-line Junction Temperature Estimation and Prognostic of SiC Power Modules," in *2018 IEEE Energy Conversion Congress and Exposition (ECCE)*, Sep. 2018, pp. 1907–1913.

[10] L. Zhang, X. Yuan, X. Wu, C. Shi, J. Zhang and Y. Zhang, "Performance Evaluation of High-Power SiC MOSFET Modules in Comparison to Si IGBT Modules," in *IEEE Transactions on Power Electronics*, vol. 34, no. 2, pp. 1181-1196, Feb. 2019.

[11] O. Alavi, M. Abdollah, and A. H. Viki, "Assessment of thermal network models for estimating IGBT junction temperature of a buck converter," in *2017 8th Power Electronics, Drive Systems Technologies Conference (PEDSTC)*, Feb. 2017, pp. 102–107.

[12] A. S. Bahman, K. Ma, and F. Blaabjerg, "Thermal impedance model of high power IGBT modules considering heat coupling effects," in *2014 International Power Electronics and Application Conference and Exposition*, Nov. 2014, pp. 1382–1387.

[13] C. Sintamarean, F. Blaabjerg and H. Wang, "A novel electro-thermal model for wide bandgap semiconductor based devices," *2013 15th European Conference on Power Electronics and Applications (EPE)*, Lille, France, 2013, pp. 1-10.

[14] Datasheet FF400R07A01E3_S6 IGBT Power Module. URL: https://www.infineon.com/dgdl/Infineon-FF400R07A01E3_S6-DataSheet-v03_04-EN.pdf?fileId=5546d46262b31d2e016301931a14339a

[15] C. Fang, T. An, F. Qin, X. Bie, and J. Zhao, "Study on temperature distribution of IGBT module," in *2017 18th International Conference on Electronic Packaging Technology (ICEPT)*, Aug. 2017.

[16] O. Olanrewaju, Z. Yang, N. Evans, A. Fayyaz, T. Lagier, and A. Castellazzi, "Investigation of Temperature Distribution in SIC Power Module Prototype in Transient Conditions," in *2019 20th International Symposium on Power Electronics (Ee)*, Oct. 2019, pp. 1–5.

[17] Y. Avenas, L. Dupont and Z. Khatir, "Temperature Measurement of Power Semiconductor Devices by Thermo-Sensitive Electrical Parameters—A Review," in *IEEE Transactions on Power Electronics*, vol. 27, no. 6, pp. 3081-3092, June 2012.

[18] F. Stella, G. Pellegrino and E. Armando, "Three-phase SiC inverter with active limitation of all MOSFETs junction temperature," *Microelectronics Reliability*, Jul. 2020.

[19] F. Stella, P. Pescetto and G. Pellegrino, "E-Drive SiC MOSFET Inverter with Self Calibrating VON-based Junction Temperature Estimator," *2021 IEEE Energy Conversion Congress and Exposition (ECCE)*, Vancouver, BC, Canada, 2021, pp. 4731-4736.

[20] P. Pescetto, E. Armando and G. Pellegrino, "Commissioning and Sensorless Control of High Power SyR Machine Prototypes," *2019 IEEE 10th International Symposium on Sensorless Control for Electrical Drives (SLED)*, Turin, Italy, 2019, pp. 1-6.

[21] T. Söderström and P. Stoica, *"System Identification"*. Hemel Hempstead, U.K.: Prentice-Hall, 1989.

[22] F. Stella, G. Pellegrino, E. Armando, and D. Daprà, "Online Junction Temperature Estimation of SiC Power MOSFETs Through On-State Voltage Mapping," IEEE Transactions on Industry Applications, vol. 54, no. 4, pp. 3453–3462, Jul. 2018.

[23] H. Luo, F. Iannuzzo, F. Blaabjerg, M. Turnaturi, and E. Mattiuzzo, "Aging precursors and degradation effects of SiC-MOSFET modules under highly accelerated power cycling conditions," in 2017 IEEE Energy Conversion Congress and Exposition (ECCE), Oct. 2017.

[24] C. Herold, J. Sun, P. Seidel, L. Tinschert, and J. Lutz, "Power cycling methods for SiC MOSFETs," in 2017 29th International Symposium on Power Semiconductor Devices and IC's (ISPSD), May 2017.